Thermoelectric properties of the electron-doped perovskites $Sr_{1-x}Ca_xTi_{1-y}Nb_yO_3$

J. Fukuyado and K. Narikiyo
Department of Electrical and Electronics Engineering, Kagoshima University, 1-21-40 Korimoto, Kagoshima 890-0065, Japan

M. Akaki and H. Kuwahara
Department of Physics, Sophia University, Chiyoda, Tokyo 102-8554, Japan

T. Okuda
Department of Nano-structures and Advanced Materials, Kagoshima University, 1-21-40 Korimoto, Kagoshima 890-0065, Japan

(Received 19 July 2011; revised manuscript received 13 January 2012; published 10 February 2012)

We have investigated thermoelectric (TE) properties for single crystals of perovskites $Sr_{1-x}Ca_xTi_{1-y}Nb_yO_3$ for $0 \leqslant x \leqslant 0.4$ and $0 \leqslant y \leqslant 0.03$ below room temperature (RT). We found that $SrTi_{0.99}Nb_{0.01}O_3$ shows a large power factor at low temperature ($PF = 50\ \mu W/K^2$ cm at 100 K $\sim 90\ \mu W/K^2$ cm at 50 K) and the largest dimensionless TE figure-of-merit below 40 K ($ZT \sim 0.07$) among the ever-reported materials. Such a large low-temperature TE response around a carrier concentration of 10^{20} cm^{-3} is due to a distinct electron-phonon interaction, which could relate to the superconducting state. We also found that the Ca^{2+} substitution for Sr^{2+} increases ZT at 300 K for $Sr_{1-x}Ca_xTi_{0.97}Nb_{0.03}O_3$ from 0.08 to 0.105. The enhancement of ZT around RT originates both in a large reduction of a thermal conductivity due to an introduced randomness into the crystal structure and in an unexpected enhancement of a Seebeck coefficient.

DOI: 10.1103/PhysRevB.85.075112 PACS number(s): 72.15.Jf, 71.20.−b, 65.40.Ba, 74.62.Dh

I. INTRODUCTION

Technology of mutual conversion between electric and thermal energy by using a thermoelectric (TE) property of a material is one of the key technologies for energy and environment problems. The TE performance of a material is expressed by a dimensionless TE figure-of-merit ZT,[1] where $Z = S^2/\rho\kappa = S^2\sigma/\kappa$ and S, ρ, σ, κ, and T are Seebeck coefficient, electric resistivity, electric conductivity, thermal conductivity, and absolute temperature, respectively. The maximum efficiencies of Peltier device and TE electric generator monotonically increase with the increase of ZT.[1] However, finding a material with a large ZT value is quite difficult[1] because the physical properties included in Z are correlated with each other.

Since a good TE property was found in Na_xCoO_2,[2] transition-metal oxides (TMOs) have been attracted and widely investigated as a good TE material, replacing the known TE materials, because of its abundance, stability, and environmental benignant. Several bulk Co oxides show good p-type TE properties [single crystal: $ZT = 1 \sim 2.5$;[3] polycrystal: $ZT = 0.3 \sim 0.8$ (Refs. 4 and 5)] compatible with the TE inorganic semiconductors, and some bulk n-type oxides, such as ZnO,[6] $SrTiO_3$,[7,8] and $CaMnO_3$,[9] are known to have a potential of a good n-type TE material.

Perovskite $SrTiO_3$ with a cubic structure [Fig. 1(a)] is one of the prototype TMOs. While $SrTiO_3$ is often used as an oxide electronic material, it shows various unusual phenomena such as superconductivity,[10,11] quantum ferroelectricity,[12,13] anomalous photoconductivity,[14] and large n-type TE response.[7] In order to investigate these phenomena in $SrTiO_3$, the effects of various substitutions have been widely investigated. Among them, the substitution of Ca^{2+} for Sr^{2+} was reported to induce structural transitions and to dramatically affect the dielectric properties.[15,16] Since the ionic radius of the Ca^{2+} ion is much smaller than that of the Sr^{2+} ion, the Ca substitution lowers the crystal symmetry from cubic to orthorhombic ones and gives rise to a complex structural and dielectric phase diagram of $Sr_{1-x}Ca_xTiO_3$.[15,16]

In this paper, we tried to improve the TE properties of $SrTiO_3$ below room temperature (RT) by the Ca substitutions for Sr in the lightly electron-doped $SrTi_{1-y}Nb_yO_3$. We expected that the randomness introduced into the structure and the lowering of the crystal symmetry by the Ca substitution effectively reduce κ and consequently increase ZT below RT. In this study, we found that $SrTi_{0.99}Nb_{0.01}O_3$ shows the largest ZT below 40 K among the ever-reported materials and that ZT for $Sr_{1-x}Ca_xTi_{0.97}Nb_{0.03}O_3$ around RT is enhanced from 0.08 to 0.105 by the Ca substitution. We will discuss the origins of such relatively good low-T TE properties for single crystals of the electron-doped perovskites $Sr_{1-x}Ca_xTi_{1-y}Nb_yO_3$ for $0 \leqslant x \leqslant 0.4$ and $0 \leqslant y \leqslant 0.03$ by using various experimentally determined physical quantities.

II. EXPERIMENTAL PROCEDURE

Polycrystalline powder $Sr_{1-x}Ca_xTi_{1-y}Nb_yO_3$ was first prepared by a solid-state reaction of starting materials of $SrCO_3$, $CaCO_3$, TiO_2, Ti, and Nb_2O_5. A stoichiometric mixture of the starting materials was first ground and sintered at 1000 °C for 12 h in air. After the pre-reaction, the obtained sample was again ground and sintered at 1300 °C in air. Then, the obtained powder was pressed into a rod with a size of 4–5 mm in diameter and 50–80 mm in length and was sintered at 1350 °C for 5 h. By using the obtained polycrystalline rod, single crystals of $Sr_{1-x}Ca_xTi_{1-y}Nb_yO_3$ were melt-grown by a floating zone (FZ) method at a feeding speed of 20–30 mm/h in flow of pure Ar gas. The 3% Nb substitutions for Ti are near the solid-solubility limit in $Sr_{1-x}Ca_xTiO_3$ single crystal grown by the FZ method, so in this paper we confine the arguments to $y \leqslant 0.03$. To characterize the crystal, powder

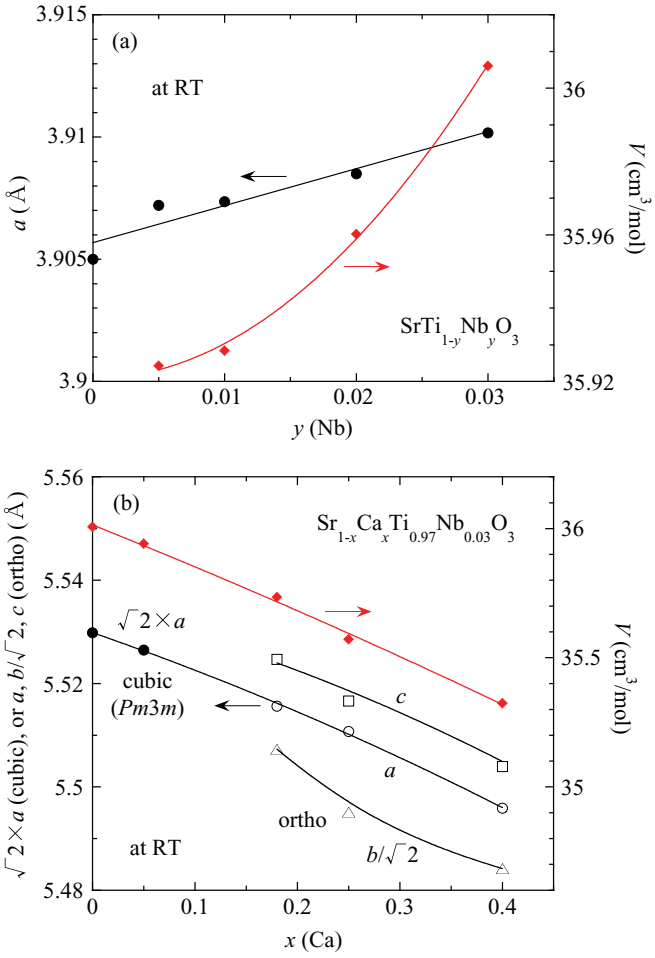

FIG. 1. (Color online) Lattice parameters for (a) $SrTi_{1-y}Nb_yO_3$ and (b) $Sr_{1-x}Ca_xTi_{0.97}Nb_{0.03}O_3$ single crystals. Solid lines are guides to the eye.

x-ray-diffraction (XRD) and energy-dispersive x-ray (EDX) analyses measurements were carried out at RT. The ρ was measured by a conventional four-probe method and the κ and S were simultaneously measured by a steady-state method. The carrier concentration (n) at RT was determined by a measurement of Hall coefficient (R_H) under magnetic fields of ± 7 T. The specific-heat measurement was done by using a relaxation method.

The XRD measurements indicate that all crystals are single phase without impurities within resolutions. Figures 1(a) and 1(b) show the Nb (y) and Ca (x) doping dependences of lattice parameters and volume deduced from the Rietveld analysis of the powder XRD patterns. As shown in Fig. 1(a), the lattice parameter (a) and volume (V) for cubic $SrTi_{1-y}Nb_yO_3$ with a space group of $Pm3m$ (No. 221) monotonically increase with the increase of y. The compositions deduced from the EDX measurements are identical to the prescribed ones within experimental errors, and the n determined from the measurements of R_H are almost consistent with the nominal ones ($n_{\rm nominal}$) (Table I). However, the n for orthorhombic $Sr_{1-x}Ca_xTi_{0.97}Nb_{0.03}O_3$ is clearly smaller than the $n_{\rm nominal}$ (Table II), although the lattice parameters (a, b, and c) and V for $Sr_{1-x}Ca_xTi_{0.97}Nb_{0.03}O_3$ deduced on the assumption of a space group of $Pmna$ (No. 62) (Ref. 17) monotonically decrease with an increase of x [Fig. 1(b)], and the EDX measurements indicate the nearly nominal compositions within experimental errors. The cations in $Sr_{1-x}Ca_xTi_{0.97}Nb_{0.03}O_3$ may be partially separated, leading to deficiencies of cations, which may suppress the electron doping.

III. RESULTS AND DISCUSSIONS

A. Thermoelectric properties of the lightly Nb-doped $SrTiO_3$ below room temperature

1. *Large thermoelectric properties at low temperature for $SrTi_{1-y}Nb_yO_3$*

In the first place, we discuss the Nb substitution (y) dependence of TE properties for single crystals of $SrTi_{1-y}Nb_yO_3$. Figures 2(a), 2(b), and 2(c) show temperature (T) dependences of ρ, S, and κ for $SrTi_{1-y}Nb_yO_3$ single crystals for $y \leqslant 0.03$. As shown in Fig. 2(a), the ρ dramatically decreases with the slight substitution of Nb^{5+} for Ti^{4+}. The ρ is nearly proportional to T^2 below 100 K down to about 30 K [the inset of Fig. 2(a)] and the T^2 coefficient (A) also monotonically decreases with the increase of y (Table I), as observed in the previous paper.[7] However, the ρ deviates from the T^2 dependence at the lower temperature below 30 K.[7] As shown in Fig. 2(b), the sign of S is negative and the absolute value of S as well as ρ monotonically decreases with the increase of y, indicating the electron doping by the Nb substitution. The S shows a broad peak structure around 50 K, which becomes more distinct as the carrier concentration (n) decreases. This

TABLE I. Carrier (electron) concentration (n) dependences of various physical quantities for $SrTi_{1-y}Nb_yO_3$ single crystals: $n_{\rm nominal}$ is the nominal electron density, n is the electron density determined by the Hall measurements at 300 K, $\mu_{\rm Hall}$ is the mobility at 300 K, A is the T^2 coefficient of resistivity, γ is the electronic specific-heat coefficient, β and δ are the T^3 and T^5 coefficients of low-T specific heat, m^* is the effective mass of electron, m_0 is the mass of bare electron, T_F is the Fermi temperature, and Θ_D is the Debye temperature.

y	$n_{\rm nominal}$ $\rm cm^{-3}$ $\times 10^{20}$	n $\rm cm^{-3}$ $\times 10^{20}$	$\mu_{\rm Hall}$ cm/Vs	A Ω cm/K^2 $\times 10^{-8}$	γ J/K^2 mol $\times 10^{-3}$	β J/K^3 mol $\times 10^{-5}$	δ J/K^4 mol $\times 10^{-7}$	A/γ^2 * $\times 10^{-2}$	m^*/m_0	T_F K	Θ_D K
0.005	0.838	0.65	6.89	8.31							
0.01	1.68	1.71	6.88	3.67	1.55	4.59	2.76	1.53	2.32	271	327
0.02	3.35	2.75	8.48	2.28							
0.03	5.02	5.48	6.88	1.63	2.27	4.48	2.25	0.316	2.30	593	304

*$(\Omega$ cm/K$^2)/($J/K^2 mol$)^2$

TABLE II. Ca-doping (x) dependences of various physical quantities for $Sr_{1-x}Ca_xTi_{0.97}Nb_{0.03}O_3$ single crystals. The symbols are the same as those in Table I.

x	n_{nominal} cm^{-3} $\times 10^{20}$	n cm^{-3} $\times 10^{20}$	μ_{Hall} cm/Vs	A Ω cm/K^2 $\times 10^{-8}$	γ J/K^2 mol $\times 10^{-3}$	β J/K^3 mol $\times 10^{-5}$	δ J/K^4 mol $\times 10^{-7}$	A/γ^2 * $\times 10^{-2}$	m^*/m_0	T_F K	Θ_D K
0	5.02	5.48	6.88	1.63	2.27	4.48	2.25	0.316	2.30	593	304
0.05	5.02	4.59	7.83	1.54							
0.18	5.05	4.44	6.24	1.74	2.13	6.94	2.36	0.383	2.33	508	349
0.25	5.08	4.1	4.96								
0.4	5.11	3.72	3.90	3.27							

*$(\Omega\ \text{cm/K}^2)/(\text{J/K}^2\ \text{mol})^2$

enhancement of S around $\Theta_D/5$ [Θ_D: Debye temperature deduced from the specific-heat measurement (Table I)] is due to a phonon drag effect,[7] which will be discussed later. On the other hand, the κ is suppressed by the slight substitution of Nb for Ti, indicating that the κ is effectively reduced by the randomness introduced into the Ti site by the partial substitution of Nb.

Figures 3(a) and 3(b) show T dependences of power factors ($PF = S^2/\rho$) and dimensionless TE figure-of-merits ($ZT = S^2T/\rho\kappa$) of $SrTi_{1-y}Nb_yO_3$ for $y \leqslant 0.03$. Around RT, the PF value monotonically increases with the increase of y and becomes about 26 μW/K^2 cm at 300 K for $y = 0.03$ [Fig. 3(a)], which is comparable to that for Bi_2Te_3.[18] Since

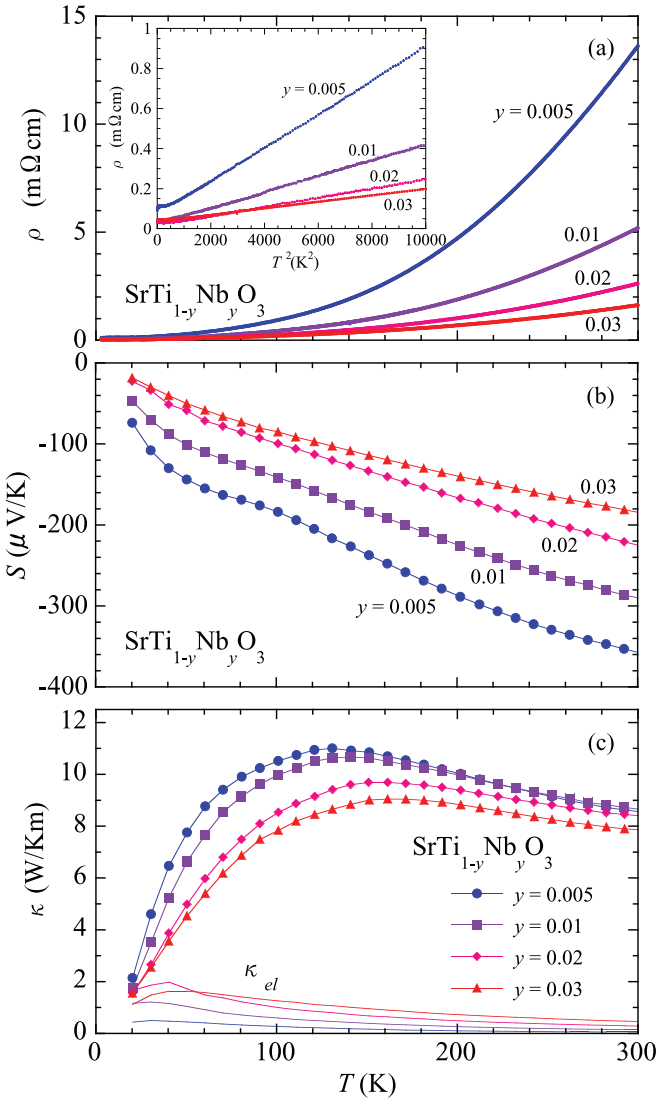

FIG. 2. (Color online) Temperature (T) dependences of (a) resistivity (ρ), (b) Seebeck coefficient (S), and (c) thermal conductivity (κ) for $SrTi_{1-y}Nb_yO_3$ single crystals for $y \leqslant 0.03$. Solid lines in (c) denoted by κ_{el} express electronic contributions to κ deduced by the Wiedemann-Franz law.

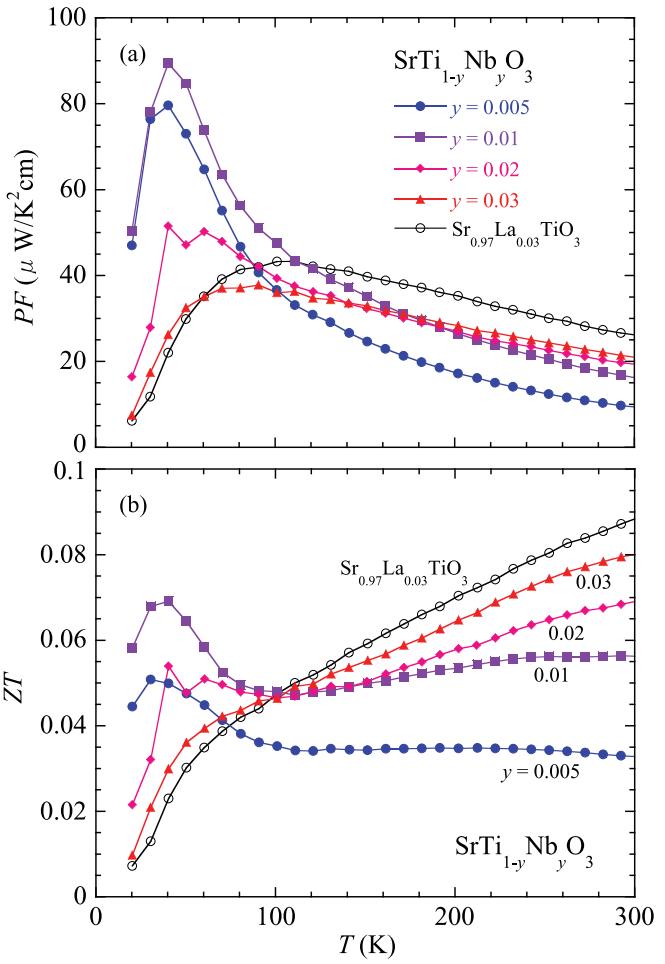

FIG. 3. (Color online) T dependences of (a) power factors (PF) and (b) dimensionless thermoelectric figure of merits (ZT) for $SrTi_{1-y}Nb_yO_3$ single crystals, together with those of $Sr_{0.97}La_{0.03}TiO_3$ single crystal.

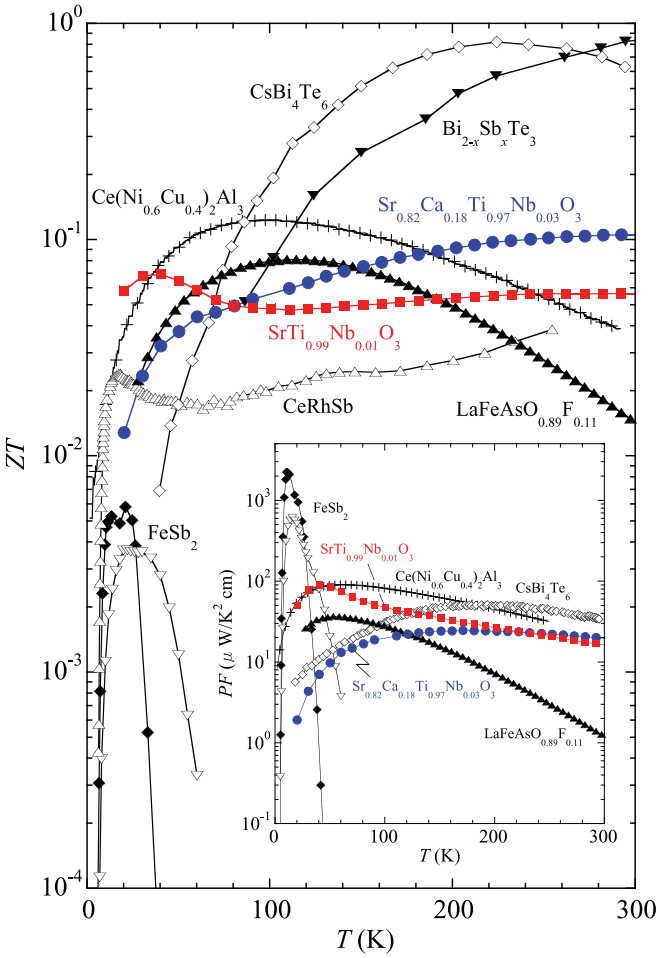

FIG. 4. (Color online) Comparison of ZT below 300 K for $SrTi_{0.99}Nb_{0.01}O_3$ and $Sr_{0.82}Ca_{0.18}Ti_{0.97}Nb_{0.03}O_3$ with those for typical low-T TE materials: p-type $Bi_{2-x}Sb_xTe_3$ (Ref. 18), p-type $CsBi_4Te_6$ (Ref. 18), p-type CeRhSb (Ref. 19), p-type $FeSb_2$ (Ref. 20), p-type $Ce(Ni_{0.6}Cu_{0.4})_2Al_3$ (Ref. 21), and n-type $LaFeAsO_{0.89}F_{0.11}$ (Ref. 22). The inset shows T dependences of PF below room temperature for these materials.

the κ is suppressed by the Nb substitution [Fig. 2(c)], the ZT around RT largely increases with the increase of y and becomes about 0.08 at 300 K for $y = 0.03$ [Fig. 3(b)].

On the other hand, at the lower temperature below 100 K, the PF value is much enhanced around $y = 0.01$ and becomes about 90 $\mu W/K^2$ cm at 40 K for $y = 0.01$, which is similar to that observed in $Sr_{1-x}La_xTiO_3$ (about 65 $\mu W/K^2$ cm[7] at 60 K for $x = 0.014$). The quite large PF apparently originates in the distinct phonon drag effect on S in the low-n region. Consequently, the ZT value for $SrTi_{0.99}Nb_{0.01}O_3$ becomes about 0.07 at 40 K. As shown in Fig. 4, the observed ZT value at low temperature for $SrTi_{0.99}Nb_{0.01}O_3$ is the largest value among the previously reported values below 40 K.

2. *Effect of the electron-phonon interaction on the low-temperature thermoelectric properties for $SrTi_{1-y}Nb_yO_3$*

In order to understand the good low-T TE property for $SrTi_{0.99}Nb_{0.01}O_3$, the n dependences of PF for $SrTi_{1-y}Nb_yO_3$ at each temperature are summarized in Fig. 5. While the PF value around RT monotonically increases with the increase of

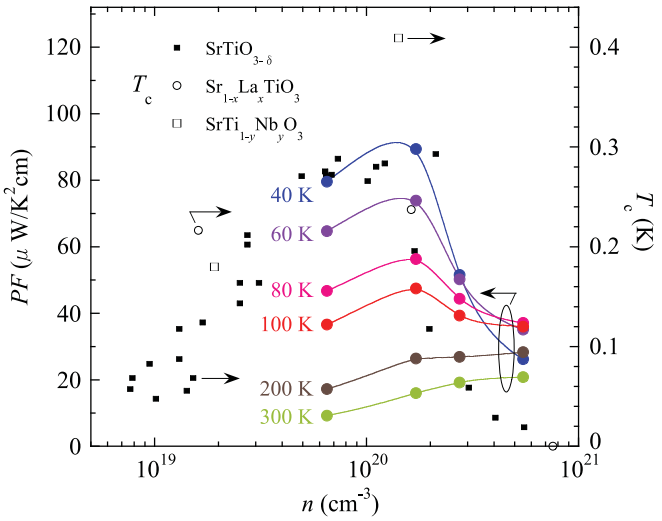

FIG. 5. (Color online) Carrier concentration (n) dependences of PF for $SrTi_{1-y}Nb_yO_3$ single crystals and those of superconducting critical temperature (T_c) for $SrTiO_{3-\delta}$, $Sr_{1-x}La_xTiO_3$, and $SrTi_{1-y}Nb_yO_3$ (Ref. 23).

n, the PF value comes to be enhanced around $n \sim 10^{20}$ cm^{-3} as the temperature decreases. The observed n dependence of PF at the lower temperature is apparently due to the enhancement of S by a phonon drag effect,[7] i.e., a kind of electron-phonon interaction. Therefore, it is interesting to compare the n dependence of PF with that of the critical temperature of superconducting transition (T_c) for the lightly electron-doped $SrTiO_3$.[23] As shown in Fig. 5, the n dependence of PF at the lower temperature quite resembles the n dependence of T_c. The fact also indicates that the origin of the good low-T TE property for the lightly Nb-doped $SrTiO_3$ could be the same one as that of the superconducting state, i.e., the distinct electron-phonon interaction.

In order to clarify the origin of the good low-T TE property further, we deduced electronic specific-heat coefficients (γ) and effective mass (m^*) by measurements of specific heat (C) and R_H. Figure 6(a) shows C/T versus T^2 for $SrTi_{0.99}Nb_{0.01}O_3$ and $SrTi_{0.97}Nb_{0.03}O_3$. As shown in Fig. 6(a), the C for both compounds can be well fitted to the formula $C/T = \gamma + \beta T^2 + \delta T^4$, where the first term of the right hand expresses the electronic specific heat, the second term expresses the phonon contribution, and the third term perhaps comes from the higher-order term of the phonon one. Table I summarizes the electronic specific-heat coefficient (γ), ratio of effective mass to bare mass of electron (m^*/m_0), and A/γ^2 for $SrTi_{1-y}Nb_yO_3$. The m^* was deduced on the base of the Boltzmann transport in a simple parabolic band with the sixfold degeneracy [$6 = 2 \times 3$: 2 comes from the spin degree of freedom and 3 from the orbital degree of freedom ($3d$ t_{2g})].[7]

The observed T dependences of S for these lightly electron-doped compounds can not be well reproduced by the Boltzmann transport model with the constant scattering parameter (r) of the energy- (ϵ-) dependent relaxation time ($\tau = \tau_0 \epsilon^{r-1/2}$). Especially for $y = 0.01$, the r estimated at each T as well as the PF largely increases with the decrease of T below 100 K, as shown in the inset of Fig. 6(a), suggesting that the relaxation time dramatically changes due to the phonon

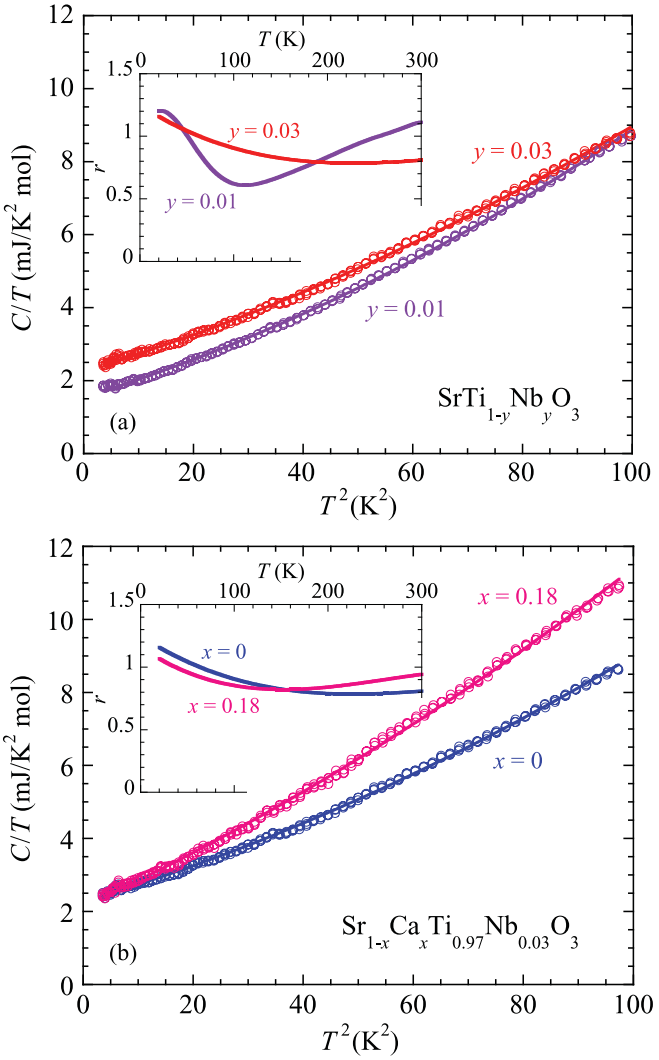

FIG. 6. (Color online) T dependences of specific heat (C) for (a) $SrTi_{1-y}Nb_yO_3$ and (b) $Sr_{1-x}Ca_xTi_{0.97}Nb_{0.03}O_3$ single crystals. The solid lines show the results of fitting to the relation $C/T = \gamma + \beta T^2 + \delta T^4$. The insets show temperature dependences of scattering parameter (r) in the energy- (ϵ-) dependent relaxation time ($\tau = \tau_0 \epsilon^{r-1/2}$) of the Boltzmann transport model with a simple parabolic band with the sixfold degeneracy deduced by using the observed Seebeck coefficient (S), electron concentration (n), and effective mass (m^*).

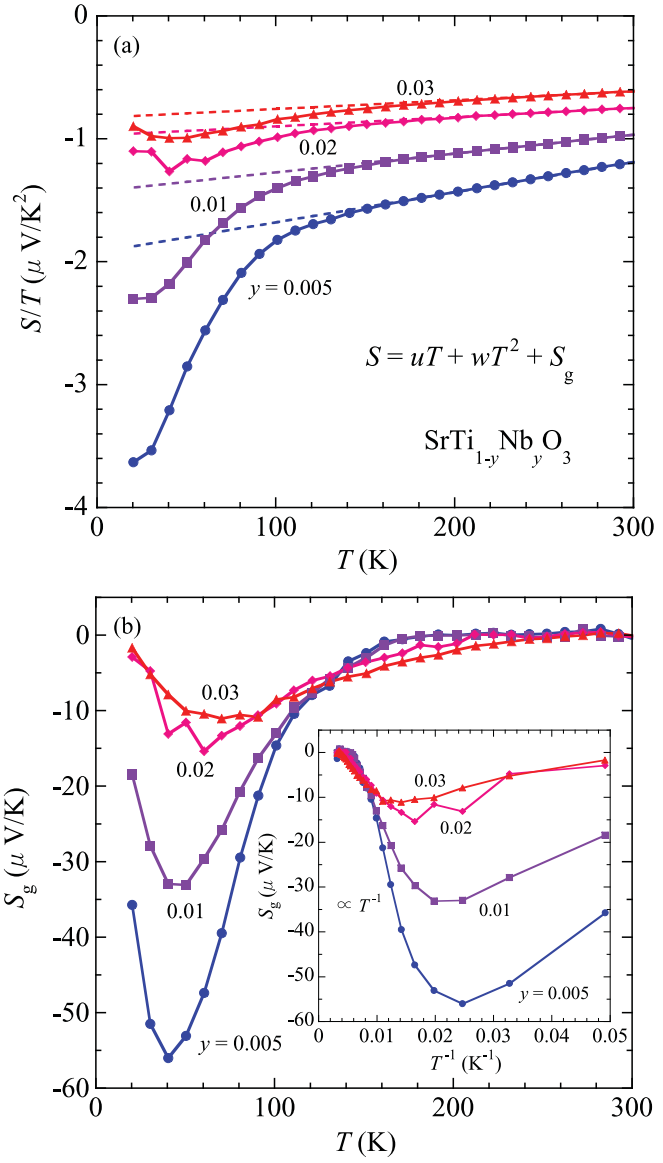

FIG. 7. (Color online) (a) T dependences of S/T for $SrTi_{1-y}Nb_yO_3$ for $y = 0.005$, 0.01, 0.02, and 0.03. The dotted lines show the results of fitting of the high-T regimes to the formula $S/T = u + wT$, where u and w are the coefficients of T and T^2 components of S, respectively. (b) T dependences of the deduced S_g for $y = 0.005$, 0.01, 0.02, and 0.03. The inset shows the S_g versus T^{-1}. S_g at high temperature seem to be proportional to T^{-1}.

drag effect, while the change of r above 100 K partially comes from the lifting of Fermi degeneracy due to the low Fermi temperature (T_F) (Table I). On the other hand, the obtained m^*/m_0 for $y \geqslant 0.01$ is almost constant ($\sim$2.3) with the variation of y within experimental errors, although the phonon drag effect becomes distinct as y decreases. Furthermore, the A/γ^2 is enhanced with the decrease of y, which is quite larger than the conventional value for Kadowaki-Woods law, which may also suggest the distinct electron-phonon interaction for $y = 0.01$ at low temperature.[7] Taking into account these results, we conclude that the observed distinct phonon drag effect enhances the S not through a change of character of Fermi surface (m^*), but through a change of relaxation time of scattering.

According to the theory[24] of phonon drag for a metal, to a first approximation, the S is expressed as follows: $S = S_d + S_g$, where S_d and S_g are the diffusion and phonon drag components, respectively. This approximation means that the momentum transfer from phonon to electron does not affect the electronic specific heat (C_{el}) mainly contributing to S_d, i.e., it can be applied, if the electron-lattice interaction little contributes to m^*. Therefore, our above conclusion supports the appliance of the approximation. In order to separate two terms, we plotted the S/T versus T as shown in Fig. 7(a) and found that the S for $SrTi_{1-y}Nb_yO_3$ is well expressed as $S = S_d + S_g = uT + wT^2 + S_g$. The observed T linear contribution (uT) is well known as a characteristic of a metal. We can deduce the electronic specific heat (C_{el}) by using the relation $S_d = C_{el}/e$ where e is elementary electric charge.

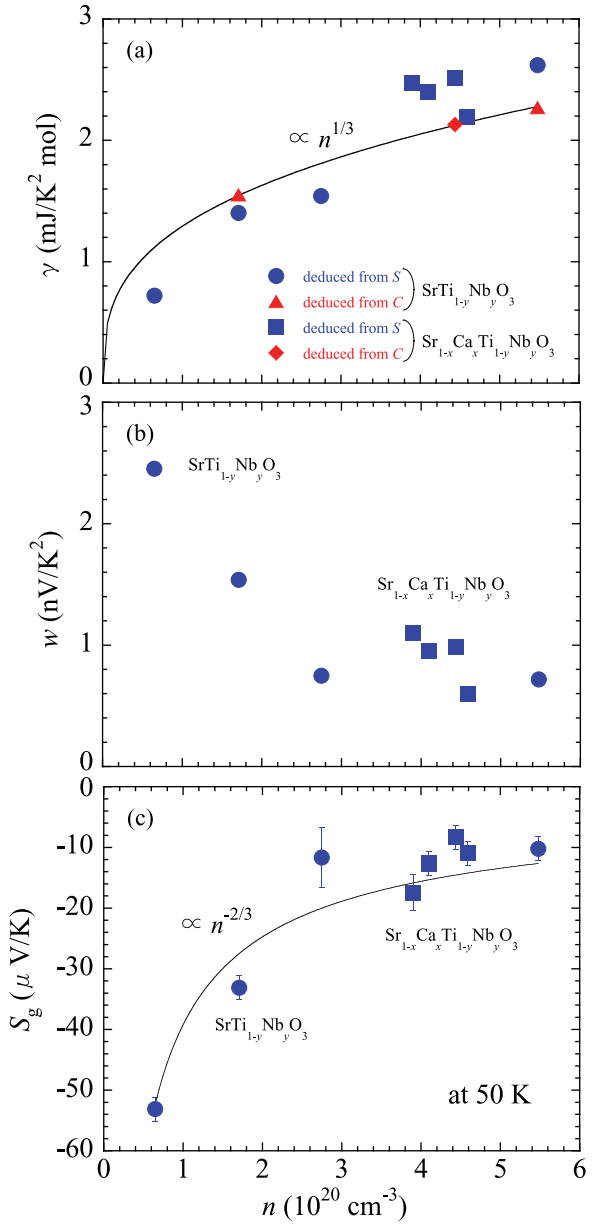

FIG. 8. (Color online) (a) Carrier concentration (n) dependences of the γ. The solid triangle and circle show the γ for $SrTi_{1-y}Nb_yO_3$ deduced from the results of C and S, respectively, while the solid diamond and square show those for $Sr_{1-x}Ca_xTi_{1-y}Nb_yO_3$ from the results of C and S, respectively. The solid line shows the result of fitting of the γ deduced from C to $\gamma \propto n^{1/3}$. (b) n dependence of the coefficient (w) of T^2 component of S. (c) n dependence of S_g at 50 K. The solid line shows the result of fitting to $S_g \propto n^{-2/3}$.

Since $C_{el} = \gamma T$, we can get $\lim_{T\to 0} S_d/T = \gamma/e$ and estimate the γ as follows: $\gamma = eu$. The estimated γ are shown in Fig. 8(a) together with those directly deduced from C_{el} [Table I and Fig. 6(a)]. There is a good consistency between the γ values deduced from C_{el} and S_d, evidencing the validity of the analysis. On the other hand, the wT^2 perhaps originates in the deviation from the T linearity coming from the lifting of Fermi degeneracy due to the low T_F, which is supported by the fact that the w coefficient dramatically decreases with the increase of n as shown in Fig. 8(b).

The residual component of S should be attributed to the phonon drag contribution (S_g). Figure 7(b) shows the deduced S_g. The component is much enhanced with the decrease of n and is nearly proportional to T^{-1} in the higher T regime [the inset of Fig. 7(b)]. These behaviors are undoubtedly the characteristics of phonon drag effect. The estimated contribution of phonon drag takes up about one third in the total S for $y = 0.01$ at 50 K, i.e., it makes the ZT for $y = 0.01$ at 50 K about 2.2 times larger.

According to the theory,[24] the phonon drag contribution is expressed as follows: $S_g \approx \frac{1}{3}\frac{C_{\rm latt}}{ne}\alpha$, where $C_{\rm latt}$ is a phonon contribution to C. The α is a probability for electron-phonon scattering among all scattering processes. The α for a typical metal is $\frac{\tau_{pp}}{\tau_{pp}+\tau_{pe}} = \frac{l_{pp}}{l_{pp}+l_{pe}}$,[24] where τ_{pp} and τ_{pe} are the relaxation time of phonon-phonon and phonon-electron scatterings, and l_{pp} and l_{pe} are the mean-free path of phonon-phonon and phonon-electron scatterings. Since the phonon-phonon scattering is dominant at high temperature, $l_{pp} \ll l_{pe}$, so $S_g \approx \frac{1}{3}\frac{C_{\rm latt}}{ne}\frac{l_{pp}}{l_{pe}}$. Furthermore, l_{pe} is nearly constant and l_{pp} is proportional to T^{-1} at high temperature, so $S_g \propto T^{-1}$ in the high-T regime. As shown in Fig. 8(c), the S_g at 50 K for $SrTi_{1-y}Nb_yO_3$ is roughly proportional to $n^{-2/3}$, which are qualitatively consistent with the above discussions (because $l_{pe} \propto n^{-1/3}$). By using the results of $C_{\rm latt}$ in Table I and Fig. 6(a), the α ($\approx \frac{l_{pp}}{l_{pe}}$) values at 50 K for $y = 0.01$ and 0.03 are estimated to be about 10^{-3}.

B. Effect of the Ca substitution for Sr on the thermoelectric properties of $Sr_{1-x}Ca_xTi_{0.97}Nb_{0.03}O_3$

Next, on purpose to reduce κ by introducing randomness into the structure and improve the TE property, we investigated the effect of substitution of Ca^{2+} for Sr^{2+} on the TE property of $SrTi_{0.97}Nb_{0.03}O_3$.

Figure 9(a) shows the T dependence of ρ for $Sr_{1-x}Ca_xTi_{0.97}Nb_{0.03}O_3$ in cubic ($x \leqslant 0.05$) and orthorhombic ($x \geqslant 0.18$) phases. The ρ around RT monotonically increases with the Ca substitution, but the increase is not dramatic even after the structural transition from cubic to orthorhombic structures around $x \sim 0.1$, leading to the enhancement of TE property by the Ca substitution. Except for $x = 0.25$, the ρ is nearly proportional to T^2 at low temperature, while the ρ-T curve for $x = 0.25$ shows a distinct hysteresis around 110 K [the inset of Fig. 9(a)], which may relate to a structural transition accompanying an antiferroelectric phase transition observed in non-Nb-doped $Sr_{1-x}Ca_xTiO_3$.[16] The γ deduced by the fitting of C to the relation $C/T = \gamma + \beta T^2 + \delta T^4$ [Fig. 6(b)] and the m^* deduced by using the γ and R_H values do not change with the Ca substitution within the experimental errors (Table II). The T^2 coefficient A of ρ does not seem to largely change with x [the inset of Fig. 9(a)], so the ratio A/γ^2 for the Ca-doped compound except for $x = 0.25$ also does not largely change by the Ca substitution within the experimental errors (Table II), which seem to indicate an absence of dramatic change of scattering mechanism.

However, as shown in Fig. 9(b), the $|S|$ increases with the increase of x. Although the deficiency of cations should suppress the electron doping and increase the $|S|$, the enhancement of S seems to be more dramatic than the

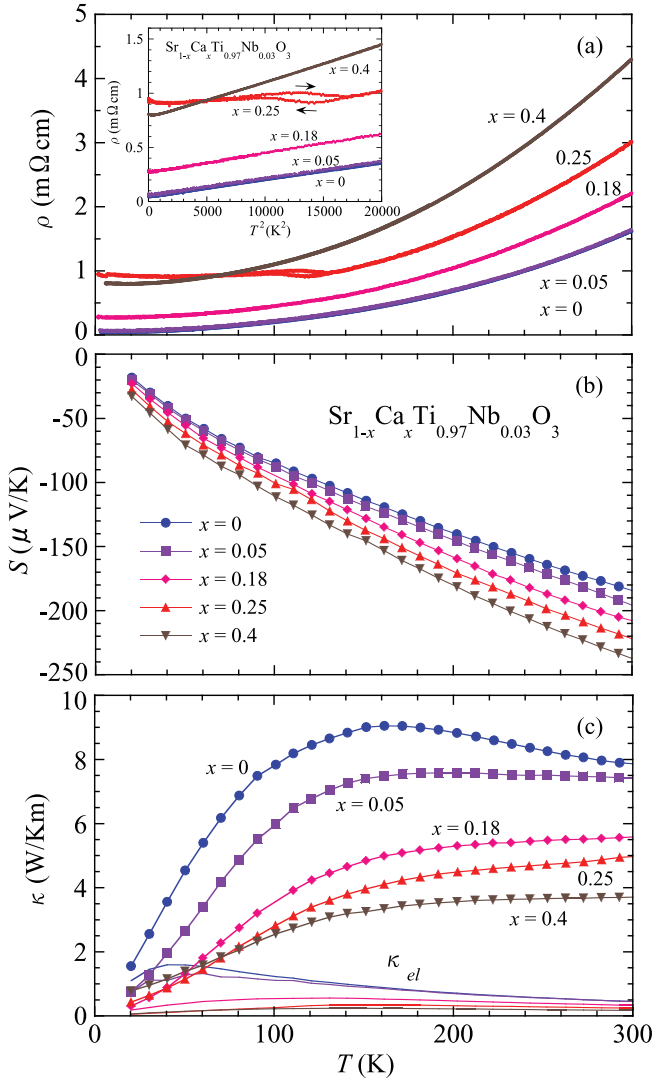

FIG. 9. (Color online) T dependences of (a) ρ, (b) S, and (c) κ for $Sr_{1-x}Ca_xTi_{1-y}Nb_yO_3$ single crystals. Solid lines in (c) denoted by κ_{el} express electronic contributions to κ deduced by the Wiedemann-Franz law.

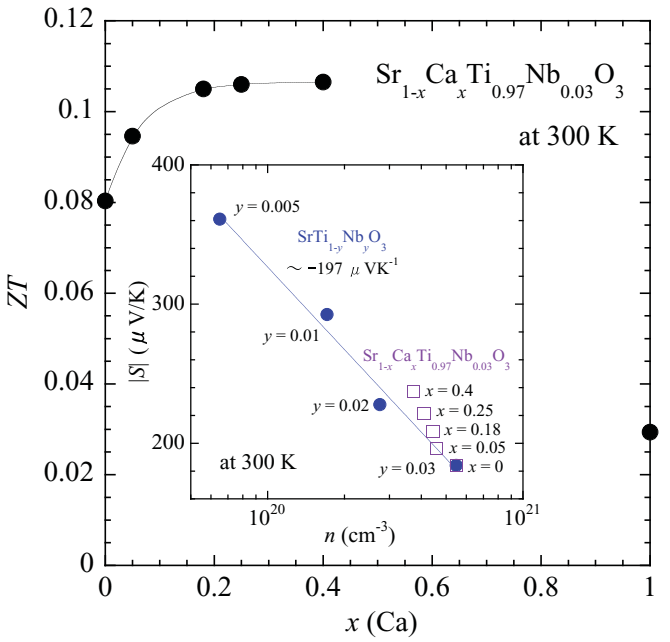

FIG. 10. (Color online) Ca-doping (x) dependence of ZT at 300 K for $Sr_{1-x}Ca_xTi_{0.97}Nb_{0.03}O_3$. The inset shows n dependences of $|S|$ at 300 K for $SrTi_{1-y}Nb_yO_3$ (solid circles) and $Sr_{1-x}Ca_xTi_{0.97}Nb_{0.03}O_3$ (open squares).

one expected from the change of n. The inset of Fig. 10 shows the n dependence of $|S|$ at 300 K for $SrTi_{1-y}Nb_yO_3$ and $Sr_{1-x}Ca_xTi_{0.97}Nb_{0.03}O_3$, where the n is directly determined by the R_H measurement. While the $d|S|/d\log_{10}n$ for $SrTi_{1-y}Nb_yO_3$ is about -197 μV/K (a solid line), which is almost identical to the value $(-(k_B/e)\cdot\ln 10 \sim -198.4$ μV/K) expected from the Boltzmann transport model with a three-dimensional (3D) parabolic band,[1,7] the increase of $|S|$ for $Sr_{1-x}Ca_xTi_{0.97}Nb_{0.03}O_3$ with the decrease of n seems to be more dramatic than $-(k_B/e)\cdot\ln 10$, indicating that the m^* or the relaxation-time change with the Ca substitution.

As mentioned before, the m^* estimated from γ does not change with the Ca substitution within the experimental errors (Table II). The scattering of data of C at the lowest T is about ± 5 % of the C value [Fig. 6(b)] and the fitting errors are less than ± 0.1%, indicating that the error of m^* should be much less than ± 5 %. Furthermore, the γ values estimated from C are well fitted to $n^{1/3}$, as shown in Fig. 8(a), which also evidences the high accuracy of the estimation of m^*. Hence, the increase of $|S|$ does not seem to be fully explained by the change of electronic state in the ground state in addition to the decrease of n due to the suppression of electron doping by the deficiency. The thermally excited state may be slightly modulated by the change of Ti $3d$ and O $2p$ hybridization[25] due to the structural change, which may lead to the larger w coefficient than the extrapolated one for non-Ca-doped compounds [Fig. 8(b)].

Another possible scenario to explain the observed systematic change of S is a slight (not dramatic) change of the relaxation time of scattering with the Ca substitution due to the change of structure and the increase of disorder originating in the mixture of Sr and Ca ions at the A site. Actually, the r at RT, estimated from S, n, and m^* on the assumption that the transport properties are explained by the Boltzmann transport model in a simplified parabolic band, seems to be enhanced with the increase of x [the inset of Fig. 6(b)]. However, taking into account the experimental errors, the scenario is also not a conclusive one.

The other possible scenario is the phase separation.[26] If we assume that the sample is macroscopically separated into the $SrTi_{0.97}Nb_{0.03}O_3$ (STNO) and $CaTi_{0.97}Nb_{0.03}O_3$ (CTNO) clusters, the observed behaviors of S may be reproduced by using the observed physical quantities of the actually grown STNO ($n \sim 5.48 \times 10^{20}$ cm^{-1}) and CTNO ($n \sim 1.96 \times 10^{20}$ cm^{-1}) single crystals and the rules for the synthesis of S in the cases of series and parallel connections as follows: $S_{\rm series} = \frac{\sum \kappa_i S_i}{\sum \kappa_i}$ and $S_{\rm parallel} = \frac{\sum \sigma_i S_i}{\sum \sigma_i}$, where the $S_{\rm series}$ and $S_{\rm parallel}$ are the synthetic S for the series and parallel connections, respectively, and the subscript i expresses each cluster. If more than one cluster of CTNO exists, estimating the $S_{\rm series}$ and $S_{\rm parallel}$ at RT to investigate the effect of phase separation on S, the $|S_{\rm series}|$ and $|S_{\rm parallel}|$ at RT inevitably become larger than the $|S|$ at RT for

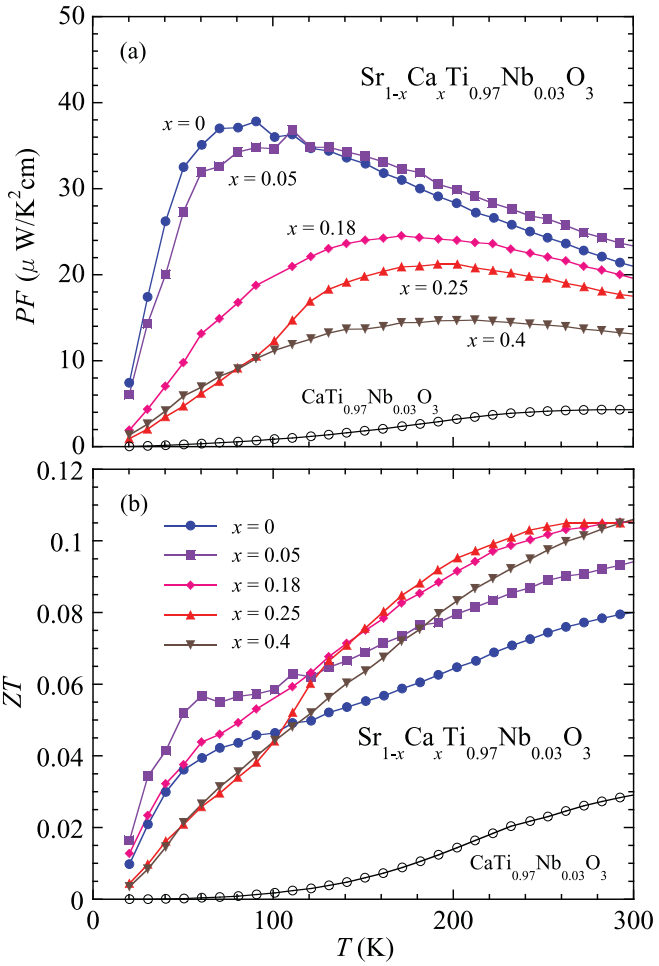

FIG. 11. (Color online) T dependences of (a) PF and (b) ZT for $Sr_{1-x}Ca_xTi_{1-y}Nb_yO_3$ single crystals. The PF and ZT for $CaTi_{0.97}Nb_{0.03}O_3$ are also shown (open circles).

STNO. It is because the $|S|$ at RT for CTNO ($\sim$278 μV/K) is about 50% larger than that for STNO ($\sim$185 μV/K) and the κ at RT for CTNO ($\sim$4.5 W/Km) is about 42% smaller than that for STNO ($\sim$7.8 W/Km), although the ρ at RT for CTNO ($\sim$21 mΩ cm) is much larger than that for STNO ($\sim$1.6 mΩ cm).

In the actual phase separation, the series and parallel connections should be randomly formed in the sample, so the total S is synthesized by the further series and parallel combinations of S_{series} and S_{parallel}. Although the synthetic $|S|$ is at least larger than that of STNO, the Ca substitution (x) dependence of S should depend upon how the clusters grow with x. The observed monotonic increase of $|S|$ with x until $x = 0.4$ seems to be able to be reproduced if the proportion of the number of CTNO clusters in the number of all clusters monotonically increases with x because the $|S_{\text{parallel}}|$ monotonically increases with the proportion. Since the actual phase-separated sample, furthermore, is more inhomogeneous than the model composed of two components, the more careful theoretical investigation is necessary to clarify if the scenario is appropriate.

On the other hand, the Ca substitution effectively reduces κ. Figure 9(c) shows the T dependences of κ for $Sr_{1-x}Ca_xTi_{0.97}Nb_{0.03}O_3$. The κ as well as σ is suppressed by the Ca substitution. The suppression of κ around RT is monotonic and seems to be independent on the structural transition, indicating that reduction of κ mainly originates in the randomness introduced into the structure by the substitution of Ca for Sr.

The T dependence of PF for $Sr_{1-x}Ca_xTi_{0.97}Nb_{0.03}O_3$ is shown in Fig. 11(a). The PF value is suppressed with the increase of x above 0.18 and the suppression is more dramatic at low temperature, which is mainly due to the increase of ρ by the Ca substitution. However, the ZT around RT [Fig. 11(b)] is enhanced due to the slight increase of $|S|$ and the large reduction of κ by the Ca substitution. The observed maximum ZT value at RT for $Sr_{1-x}Ca_xTi_{0.97}Nb_{0.03}O_3$ is about 0.105 for $x = 0.18$, 0.25, and 0.4 (Fig. 10), which is about 1.3 times larger than that for $SrTi_{0.97}Nb_{0.03}O_3$. It is noted that such an improvement of TE property has also been reported in the electron-doped perovskite manganite $Ca_{1-x}Sr_xMnO_3$ (Ref. 27) similarly due to the slight increase of $|S|$ and the large reduction of κ by the substitution at the A site. The disorder at the A site plays a crucial role for the TE property of perovskite TMOs, as similar to various layered Co oxides[28,29] in which the randomly distributed cations between the conducting layers often suppress the κ with keeping the low ρ and cause their good TE properties.

IV. SUMMARY

In this study, we have investigated thermoelectric (TE) properties for single crystals of perovskites $Sr_{1-x}Ca_xTi_{1-y}Nb_yO_3$ for $0 \leqslant x \leqslant 0.4$ and $0 \leqslant y \leqslant 0.03$ below room temperature (RT). We found that $SrTi_{0.99}Nb_{0.01}O_3$ shows the quite large power factor (PF) at low temperature ($PF =$ 50 μW/K^2 cm at 100 K $\sim$ 90 μW/K^2 cm at 50 K) and the largest dimensionless TE figure-of-merit below 40 K ($ZT \sim$ 0.07) among the ever-reported materials. Taking into account the results of specific heat and Hall coefficient measurements, such a large low-T TE response around a carrier concentration of 10^{20} cm^{-3} is due to the distinct electron-phonon interaction, which enlarges the Seebeck coefficient (S) not through an enhancement of effective mass (m^*), but through a change of relaxation time of scattering.

On the other hand, the disorder introduced by the Ca substitution for Sr in $SrTi_{0.97}Nb_{0.03}O_3$ largely increases the residual resistivity, but it slightly affects the temperature derivative of resistivity ($d\rho/dT$) and little changes the m^*. Hence, the Ca substitution does not remarkably change the ratio of the T^2 coefficient of ρ (A) to γ^2 (A/γ^2) (Table II), and it rather suppresses the PF and ZT values at low temperature. However, it enhances the ZT at RT from 0.08 to 0.105 due to the enhancement of S and the large reduction of thermal conductivity (κ) originating in the randomness introduced into the crystal structure. Although the mechanism for the enhancement of S by the A-site substitution is still an open question, the control of disorder at the A site is a promising way to improve the TE property for perovskite TMOs.

ACKNOWLEDGMENT

This work was supported by a grant-in-aid for JST-PRESTO.

[1]G. D. Mahan, Solid State Phys. **51**, 81 (1998).
[2]I. Terasaki, Y. Sasago, and K. Uchinokura, Phys. Rev. B **56**, 12685 (1997).
[3]R. Funahashi, I. Matsubara, H. Ikuta, T. Takeuchi, U. Mizutani, and S. Sodeoka, Jpn. J. Appl. Phys. **39**, L1127 (2000).
[4]R. Funahashi and M. Shikano, Appl. Phys. Lett. **81**, 1459 (2002).
[5]M. Ito, T. Nagira, D. Furumoto, S. Katsuyama, and H. Nagai, Scr. Mater. **48**, 403 (2003).
[6]M. Ohtaki, T. Tsubota, K. Eguchi, and H. Arai, J. Appl. Phys. **79**, 1816 (1996).
[7]T. Okuda, K. Nakanishi, S. Miyasaka, and Y. Tokura, Phys. Rev. B **63**, 113104 (2001).
[8]S. Ohta, T. Nomura, H. Ohta, and K. Koumoto, J. Appl. Phys. **97**, 034106 (2005).
[9]M. Ohtaki, H. Koga, T. Tokunaga, K. Eguchi, and H. Arai, J. Solid State Chem. **120**, 105 (1995).
[10]J. F. Schooley, W. R. Hosler, and M. L. Cohen, Phys. Rev. Lett. **12**, 474 (1964).
[11]C. S. Koonce, M. Marvin, M. L. Cohen, J. F. Schooley, W. R. Hosler, and E. R. Pfeiffer, Phys. Rev. B **163**, 380 (1967).
[12]J. H. Barrett, Phys. Rev. **86**, 118 (1952).
[13]K. A. Müller and H. Burkard, Phys. Rev. B **19**, 3593 (1979).
[14]T. Feng, Phys. Rev. B **25**, 627 (1982).
[15]J. G. Bednorz and K. A. Müller, Phys. Rev. Lett. **52**, 2289 (1984).
[16]R. Ranjan, D. Pandey, and N. P. Lalla, Phys. Rev. Lett. **84**, 3726 (2000).
[17]The exact space group for orthorhombic $Sr_{1-x}Ca_xTiO_3$ is controversial. In this paper, we temporarily use the space group for $CaTiO_3$ as that of orthorhombic $Sr_{1-x}Ca_xTiO_3$ to discuss the lattice parameters.
[18]D.-Y. Chung, T. Hogan, P. Brazis, M. R. Lane, C. Kannewurf, M. Bastea, C. Uher, and M. G. Kanatzidis, Science **287**, 1024 (2000).
[19]T. Takabatake, T. Sasakawa, J. Kitagawa, T. Suemitsu, Y. Echizen, K. Umeo, M. Sera, and Y. Bando, Phys. B (Amsterdam) **328**, 53 (2003).
[20]P. Sun, N. Oeschler, S. Johnsen, B. B. Iversen, and F. Steglich, J. Phys.: Conf. Ser. **150**, 012049 (2009).
[21]P. Sun, T. Ikeno, T. Mizushima, and Y. Isikawa, Phys. Rev. B **80**, 193105 (2009).
[22]T. Okuda, W. Hirata, A. Takemori, S. Suzuki, S. Saijo, S. Miyasaka, and S. Tajima, J. Phys. Soc. Jpn. **80**, 044704 (2011).
[23]H. Suzuki, H. Bando, Y. Ootuka, I. H. Inoue, T. Yamamoto, K. Takahashi, and Y. Nishihara, J. Phys. Soc. Jpn. **65**, 1529 (1996).
[24]D. K. C. Macdonald, *Principles of Thermoelectricity* (Wiley, New York, 1964).
[25]R. E. Cohen, Nature (London) **358**, 136 (1992).
[26]E. Dagotto, T. Hotta, and A. Moreo, Phys. Rep. **344**, 1 (2001).
[27]T. Okuda and Y. Fujii, J. Appl. Phys. **108**, 103702 (2010).
[28]H. W. Zandbergen, M. L. Foo, Q. Xu, V. Kumar, and R. J. Cava, Phys. Rev. B **70**, 024101 (2004).
[29]M. Roger, D. J. P. Morris, D. A. Tennant, M. J. Gutmann, J. P. Goff, J.-U. Hoffmann, R. Feyerherm, E. Dudzik, D. Prabhakaran, A. T. Boothroyd, N. Shannon, B. Lake, and P. P. Deen, Nature (London) **445**, 631 (2007).